Environmental Nanotechnology, Monitoring & Management 22 (2024) 100956

Contents lists available at ScienceDirect

Environmental Nanotechnology, Monitoring & Management

journal homepage: www.elsevier.com/locate/enmm

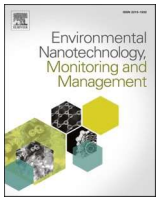

Functionalized activated carbon with whey protein amyloid fibrils for adsorption of arsenic from water

Mateo Andrés Gallardo Salas [a], Didilia Ileana Mendoza-Castillo [b,c], Adrián Bonilla-Petriciolet [c], Carlos Jiménez-Junca [a,*]

[a] Research Group in Bioprospecting, Universidad de La Sabana, Chía 250001, Colombia
[b] CONACYT, Cátedras Jóvenes Investigadores, Ciudad de México 03940, Mexico
[c] Chemical Engineering Department, Instituto Tecnológico de Aguascalientes, Aguascalientes 20256, Mexico

ARTICLE INFO

Keywords:
Adsorption
Amyloid fibrils
Arsenic
HSAB theory
Water treatment
Whey

ABSTRACT

Globally, more than 200 million people are exposed to elevated concentrations of arsenic in groundwater, thus representing an important environmental and public health problem. Apart from inorganic species, water quality suffers also from the occurrence of organic pollutants discharged by the food sector like whey, a by-product of the dairy industry. The valorisation of these organic residues is relevant to reduce water pollution and to develop new materials for different applications. This research reports the synthesis and evaluation of a novel adsorptive activated carbon composite modified with whey protein amyloids for arsenic removal from water. The adsorbent was characterized with FT-IR spectroscopy, X-ray diffraction, N_2 physisorption, pH at point of zero charge determination, and thermogravimetric analysis. Experimental adsorption kinetics and isotherms of arsenic removal were determined at optimal pH 5.0, best fitted with the PSO and Sips model, respectively. The corresponding maximum adsorption capacity for As^{5+} was 0.16 mmol g^{-1} through an endothermic process. Surface complexation was the predominant phenomenon in the adsorption mechanism as the As-O bond was formed via whey's functional groups, hydroxyl, amine, and amide, with the latter having the strong affinity to arsenate as elucidated by the HSAB theory. This study highlights the potential of whey protein as a raw material to produce added-value products and its performance as a precursor of novel adsorbents for water purification, therefore minimizing their associated disposal cost and addressing relevant environmental concerns such as arsenic contamination.

1. Introduction

Heavy metals (HMs) are systemic pollutants classed as among the most harmful environmental contaminants due to their acute toxicity, lack of biodegradation, bioaccumulation from one trophic level to another, and high mobility in various ecosystems matrices, especially water bodies (Vardhan et al., 2019; Zamora-Ledezma et al., 2021). They are found on water through natural occurrence, via lixiviation of geologically sourced minerals, and anthropogenic activities, including pesticides production, burning of fossil fuels and most importantly, mining projects. Mine effluents have been cited as one of the main sources of HMs contamination, such as gold, mercury, lead, arsenic and chromium, especially when artisanal and small-scale mining (ASGM) are involved (Marrugo-Negrete et al., 2023; Salazar-Camacho et al., 2022).

Among pollutants released from these sites, arsenic has been identified as a worldwide interest because of its hazardous nature towards public health. Arsenic is documented as a carcinogen, mutagen, and teratogen (Moreira et al., 2021), and exposure even at trace concentrations (parts-per-billion, ppb) is reported to be linked to coronary heart disease, pulmonary diseases, liver and kidney damage, hyperkeratosis and arsenicosis (Shaji et al., 2021). Besides, no alteration in odour, taste or clear appearance of water is caused by its presence. Moreover, this metalloid can exist in aquatic environments as several inorganic species depending on the chemical composition of the media: pH fluctuations, redox potential, and organic matter content (Dudek & Kołodyńska, 2022; De Oliveira et al., 2023). Arsenate (As^{5+}) is the prevalent form of arsenic on acidic and oxic conditions, which is the case for mining wastewater, and is a more thermodynamically stable state than other species like arsenite or arsine (W. Zhang et al., 2019). As such, arsenic has been regulated under the Resource Recovery and

* Corresponding author.
E-mail address: carlosjj@unisabana.edu.co (C. Jiménez-Junca).

https://doi.org/10.1016/j.enmm.2024.100956
Received 23 December 2023; Received in revised form 10 April 2024; Accepted 29 April 2024
Available online 30 April 2024

Conservation Act (RCRA-8) by the US Environmental Protection Agency (EPA) (Horne et al., 2023) and through the threshold limit of arsenic concentration in drinking water (0.01 mg L^{-1}) recommended by the World Health Organization (WHO) and adopted globally by national environmental quality legislation (Chen et al., 2016). Non-compliance of these regulations is a prime concern regarding the increasing unavailability of drinking water services free from contaminants, particularly in the Latin American context (Bundschuh et al., 2021).

A wide range of remediation approaches has been applied for arsenic removal, such as chemical precipitation (Xu et al., 2023), ion exchange (Xingfei Zhang et al., 2022), membrane technology (Emo et al., 2017), photocatalysis (Fontana et al., 2018) and biological treatment (Isabel San-Martín et al., 2023). Adsorption has been a landmark process in removing heavy metals from water because, unlike the aforementioned conventional processes, it is a highly efficient and simple operation, does not involve high operational costs related to sludge generation, and does not produce by-products that cause secondary environmental contamination (Akdemir et al., 2022; Bi et al., 2021). However, commonly used adsorbents, like activated carbon, metal oxides and activated alumina, present drawbacks related to high production costs and low selectivity for certain inorganic pollutants, despite exhibiting high surface area, small particle sizes and free valences, properties suited for adsorptive removal. This has led researchers to develop composite materials using conventional adsorbents as hosts for active ligands obtained from naturally available, low-cost sources (Tan et al., 2020a; Yanti et al., 2023). Biosorbents prepared via this intensified process possess functional groups, e.g., carboxyl, hydroxyl, carbonyl, and amino groups, that bind to heavy metals due to chemical bonding (surface complexation) and/or physical interactions (electrostatic forces, hydrogen bonding, and hydrophobic interactions) (Bucatariu et al., 2019; Mariana et al., 2021), coupled with a relatively high surface area, porosity, physical and thermal stability, and micropore and mesopore presence (Mendoza-Castillo et al., 2016; Saghir et al., 2022), resulting in a stable synergetic structure with high adsorption capacities.

In recent years, animal and plant-derived proteins have gained interest as objects of research in the field of adsorption owing to their biocompatibility, non-toxicity, and binding capacities with a widespread of pollutants. Amid this innovative approach, amyloid fibrils have proven to have special affinity for heavy metals, as initially seen regarding their role in certain neurological disorders; arsenic exposure from contaminated drinking water is associated to amyloid plaques generation, which relates to Parkinson's and Alzheimer's disease (Haidar et al., 2023). Protein amyloids are nanoscale long unbranched fibrils that have a cross-β-structure formed upon a nucleated growth process; the protein loses its native conformation via physical or chemical-induced denaturation, aggregated nuclei assemble and then initiate the exponential growth leading to the formation of oligomers, protofibrils and, ultimately, fibrils-supported by van der Waals and hydrogen bonds (Hassan et al., 2022; Sharma et al., 2023). The fibrillation process comprises a heat treatment above the proteins denaturation temperature (>75 °C) under acidic conditions far from their isoelectric point (pH < 3.5) and at several hours of incubation (Khalesi et al., 2021). This structure exhibits high chemical, mechanical and biological stability (Lutter et al., 2021), and has a larger surface area than native proteins (Peydayesh & Mezzenga, 2021). In this sense, whey protein has the potential to produce amyloids as it is composed of a wide range of quaternary proteins, particularly β-lactoglobulin (β-Lg, 17 kDa), α-lactalbumin (α-La, 14 kDa), and bovine serum albumin (BSA, 65 kDa) (Ouyang et al., 2023). Moreover, it is highly available by recovering and revaluing it from the dairy industry, where it is normally discharged to water bodies as an undesirable by-product of cheese production; currently, only 50 % is treated and transformed into different food and feed products (Mollea et al., 2013; Peydayesh & Mezzenga, 2021). Worldwide production of cheese registers approximately 24,000 kton per year (Lopes et al., 2019), which accounts for 196 Mm^3 of whey (9 L of whey are obtained for every kg of cheese produced) that pose a significant water quality problem because of its elevated chemical and biochemical oxygen demand (Lappa et al., 2019).

Researchers have developed a variety of novel materials through different synthesis routes for the treatment of arsenic-bearing water. For instance, arsenate adsorption was evaluated by Ciopec et al. (2021) using two iron-doped materials supported by oxidized and unoxidized cellulose fibres, which exhibited a higher adsorption capacity than the oxidized sample. Mladin et al. (2022) also synthesized an iron-based composite (SiO_2/Fe(acac)$_3$/NaF) via the sol–gel method capable of capturing arsenic from aqueous solutions and real groundwater containing other relevant inorganic species. Merodio-Morales et al. (2020) reported that functionalization of avocado seeds chars with lanthanum and cerium enhanced surface area and microporosity and thus, increased arsenate uptake from water. Likewise, several studies have demonstrated the successful application of whey proteins-derived amyloid fibrils for the preparation of adsorbents for heavy metal remediation. Wei et al. (2022) prepared polyethyleneimine-based aerogels embedded with BSA amyloid fibrils, obtained though ethanol-thermal denaturation, for removing copper (Cu) from water, showing a maximum adsorption capacity of 1.29 mmol g^{-1} under optimal conditions. Fan et al. (2022) also investigated Cu adsorption by amyloid fibrils, but with β-Lg as a precursor and via in-situ thermal synthesis. In addition, there has been a trend on using activated carbon (AC) as a host for fibrils from different protein sources. Sunflower and peanut self-assembled amyloids were incorporated in AC by Soon et al. (2022) and used for platinum (Pt), chromium (Cr), and lead (Pb) removal from aqueous solutions to obtain drinkable water according to WHO standards. Bolisetty & Mezzenga (2016) evaluated the heavy metal adsorption capacity of a hybrid membrane of activated carbon and β-Lg fibrils for palladium (Pd), silver (Ag), gold (Au), nickel (Ni), and aluminium (Al), which reflects whey proteins adsorption versatility for different HMs. Recently, Ramírez-Rodríguez et al. (2020) assessed the removal performance of a whey fibrils-AC composite on the purification of water polluted by mercury (Hg) and Cr. It is worth to note that the general approach for protein fibrillation and subsequent material functionalization relies on a single native isolated protein, whereas whey protein is a source of numerous proteins proven to form fibrils and thus, costs and operational efforts for protein extraction and isolation are avoided. Furthermore, these findings suggest that the high concentration of nitrogen and oxygenated functional groups of whey would lead to a favourable adsorption of arsenic, a pollutant yet to be evaluated by this type of novel materials.

In this work, the use of a composite of activated carbon functionalized with whey protein amyloid fibrils to adsorb As^{5+} from aqueous solutions is reported. Lack of proper valorisation routes for whey presents the opportunity to use it as a feedstock for low-cost sustainable materials aimed to reduce water pollution by HMs and address the water disposal problem of whey. For this purpose, the composite was characterised using various physico-chemical techniques and batch adsorption experiments at different experimental conditions were conducted to investigate the arsenic adsorption properties of the adsorbent. The nature of arsenic adsorption was studied by thermodynamic, kinetic and isotherm models, while the removal mechanisms were identified combining surface characterizations with the hard-soft acid-base (HSAB) principle.

2. Experimental

2.1. Materials

All the chemicals used in this study were reagent grade. Whey protein isolate (WPI) was obtained from IPF S.A.S. (Colombia). Commercial activated carbon (DARCO G-60) with an average particle size of 100-mesh was purchased from Sigma-Aldrich (Germany). Sodium arsenate, sodium hydroxide, hydrochloric acid, nitric acid, and potassium chloride were procured from Merck (Germany). Arsenate solutions with

different concentrations were prepared from a 13.35 mmol/L stock solution, which was obtained by dissolving the corresponding amount of arsenate salt in deionized water. This stock solution was further diluted with deionized water to obtain the adsorbate solutions used in the removal experiments.

2.2. Preparation of the adsorbent composite

Blended composite were prepared as described by Ramírez-Rodríguez et al., (2020). Initially, whey protein fibrils (WPF) were obtained by heat treatment according to the undermentioned process: a stock solution of WPI (8 wt%) was prepared by dissolving the required amount of whey in deionized water. A whey concentration of 3.8 wt% was obtained by diluting the stock solution. The initial pH of the solution was adjusted to pH 2.0 by drop-wise addition of 2.4 M HCl. Then, it was centrifuged at 9000 rpm (Thermo Fisher Scientific Sorvall ST8 FR, United States) for 30 min at room temperature (RT) and filtered through a 0.45 μm Millipore filter to remove traces of undissolved proteins. Aliquots (15 mL) of the diluted solution were heated at 74 °C for 7 h in a water bath (Memmert GmBH WNB, Germany) without stirring, and immediately cooled thereafter in an ice bath. The resultant fibrillated WPI solutions were stored at −4 °C until subsequent use. Stock solution aliquots were used as negative control experiments, since whey protein forms hydrogels at this concentration (Khalesi et al., 2021).

Then, the AC/WPF blend composite was prepared as follows: 5 g of activated carbon (AC) were dispersed in 50 mL of deionized water under continuous stirring (300 rpm) for 2 h. After homogeneity, 100 mL of whey fibril solution were added to the suspension and thoroughly mixed for 1 h. Adsorbent was fabricated by vacuum filtration of this dispersion using a vacuum pump (Vacuubrand ME 1C, Germany) and nitrocellulose filters (pore size, 0.2 mm; diameter, 47 mm; Sartorius). Film thickness was controlled by the dispersion volume being filtered (2 mL). Prior to all characterization and adsorption studies, samples were dried in an oven at 60 °C for 24 h and sieved, to homogenize their particle size (100-mesh).

2.3. Material physico-chemical characterization

Samples of modified carbon-based materials and precursors were characterized to identify structural changes due to functionalization with WPF and As^{5+} adsorption. The morphology of the adsorbent was observed by scanning electric microscopy (SEM) using a high-resolution microscope (TESCAN LYRA3, Czech Republic) with an acceleration voltage of 10 kV. Each specimen was coated with gold in vacuum before observation. Energy-dispersive X-ray spectroscopy (EDX) was utilized to detect the elemental composition of the material. Analysis of surface chemistry was performed with a Fourier Transform infrared (FT-IR) spectrometer (Thermo Fisher Scientific Nicolet iS50, Germany) within a wavenumber range of 4000–650 cm^{-1} using 32 scans per sample. Spectra were collected via pressed pellets of adsorbent samples mixed with KBr powder. X-ray diffraction (XRD) analysis was used to identify crystallographic phases of samples at room temperature in an angular range of 5-60°2θ, employing a diffractometer (Malvern-Panalytical Empyrean, United Kingdom) coupled with a PIXcel1D-Medipix3 detector, operating with Cu-Kα radiation. Collected data was identified with the HighScore Plus software and PDF2 database. Textural properties of the samples were characterized via nitrogen (N_2) adsorption–desorption method at −196 °C and increasing relative pressure from 0 to 0.96 using a surface analyser (Micromeritics 3FLEX, USA). Preliminary degassing was carried out for 6 h at 120 °C and 60 °C for AC and AC/WPF, respectively (Micromeritics Vac Prep 061, USA). The pH at point of zero charge (pH_{pzc}) was determined via the salt addition method (Azam et al., 2013): A solution of 0.01 M KCl was prepared with deionized water in a volumetric flask and used as background electrolyte. A set of aqueous solutions (40 mL) with initial pH (pH_i) ranging from 2.0 to 12.0 was prepared by adding either 0.1 M NaOH or 0.1 M HNO_3 solutions. The AC/WPF composite dose (0.02 g) was added to each KCl solution and mixed at 150 rpm for 24 h. The difference between the initial and final pH values was plotted against pH_i; the point at which the change of pH equals to zero was identified to be the pH_{pzc}. Finally, the effect of the embedded fibrils in the thermal stability of the carbonous adsorbent was evaluated by differential thermogravimetric analysis (TGA) with a simultaneous analyser (Mettler Toledo TGA/DSC 1 Star System, Sweden) over a temperature range of 25–900 °C at a heating rate of 10 °C min^{-1} and under N_2 atmosphere. Samples with a mass of ~ 8 mg were used and put into a ceramic crucible.

2.4. Batch adsorption experiments

First, batch experiments were carried out at 30 °C with As^{5+} solutions (1.33 mmol/L) to analyse the pH effect on arsenate adsorption. AC/WPF samples (0.04 g) were added to 10 mL of adsorbate solution with pH values ranging from 5.0 to 13.0. Solutions were adjusted to the desired value by adding the required amount of 1 M NaOH or 0.1 M HNO_3 and placed upon a thermo-bath (LabTech LSB-0155, Korea) at 150 rpm for 24 h. Samples were centrifuged (Hettich Tuttlingen Universal 32R, Germany) for 12 min at 6000 rpm to separate the solid–liquid phases and to determine arsenic concentrations by atomic absorption spectroscopy (Thermo Fisher Scientific iCE 3000, Germany). Adsorption capacities were calculated with the following mass balance equation (Eq. (1):

$$q_e = \frac{(C_0 - C_e)V}{m_s} \quad (1)$$

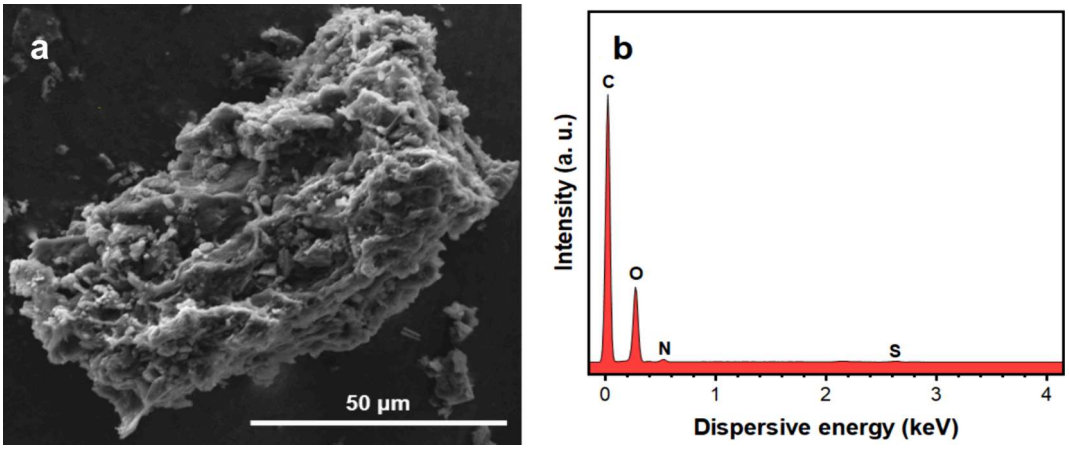

Fig. 1. (a) SEM micrograph observed at 2000X and (b) EDX pattern of AC/WPF composite.

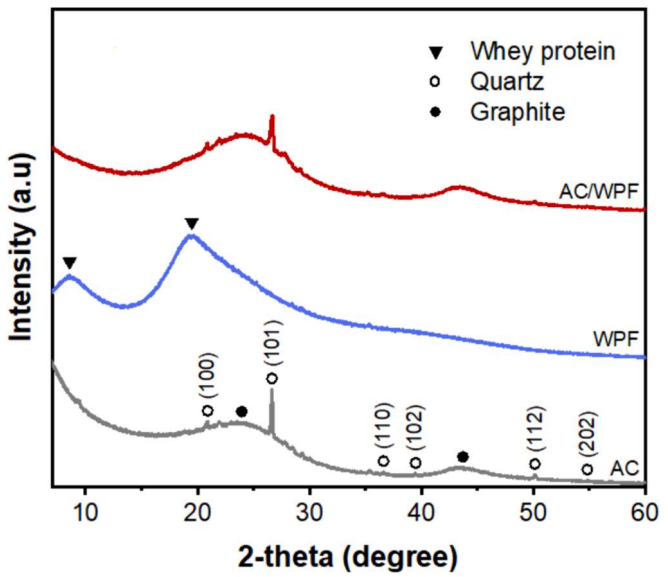

Fig. 2. X-ray diffraction patterns of activated carbon (AC), whey protein fibrils (WPF) and the hybrid material (AC/WPF).

Where C_0 and C_e are the initial and equilibrium concentrations of arsenic (mmol L^{-1}), respectively; V refers to the solution volume (L) while m_s is AC/WPF adsorbent mass (g) used in the experiments. Then, solution pH that favoured the best adsorbent performance (i.e., pH 5.0) was used to analyse the adsorption equilibrium time and maximum adsorption capacity of the prepared composite.

For kinetic experiments, two initial arsenic concentrations were evaluated (1.33 and 3.34 mmol/L) at pH 5.0, while other operational conditions remained unchanged (adsorbent dosage of 4 g/L, 30 °C, 150 rpm shaking speed). Samples were withdrawn from the thermal bath at given time intervals (0.5–24 h). The pseudo-first order (PFO), pseudo-second order (PSO), and Elovich models (see supplementary material Table S1) were employed to calculate the adsorption kinetic constants and to model the experimental data. Model suitability was evaluated by the determination coefficient (R^2), sum of squared errors (*SSE*) and Chi-square test (χ^2).

For the adsorption equilibrium study, initial arsenate concentrations of 0.27–5.34 mmol/L were used to quantify the isotherms at 20, 30 and 40 °C, respectively. Assessment of experimental data fit to theoretical isotherm models (Langmuir, Freundlich, Sips and Dubinin-Radushkevich) (Table S2) was explored via non-linear regression analysis and using the same error statistical metrics as the kinetic experiments. Data correlation of both kinetic and equilibrium studies was done with the add-in solver tool of MS Excel (Microsoft, USA). Simultaneous adsorption of arsenic and lead was evaluated using binary solutions with initial arsenic concentration of 0.66 mmol/L and lead concentrations of 0.66–1.33 mmol/L. For the influence of common co-existing anions, concentrations of Na^+ and Ca^{2+} ranged from 0.66 to 1.33 mmol/L. All adsorption experiments were performed by triplicate, including as well a blank to ensure data reproducibility.

3. Results and discussion

3.1. Characterization of raw and blended materials

The microstructure and morphology of the produced composite were studied by SEM as seen in Fig. 1a. AC/WPF showed an heterogenous rough surface with numerous pores of different sizes, intrinsic of carbonous materials, as evidenced by Zaidi & Sorokhaibam, (2021). Although amyloid fibrils are difficult to distinguish by observing the surface morphology, the EDX analysis confirms that the energy spectrum of nitrogen and sulphur can be detected in the composite system (Fig. 1b), demonstrating successful adhesion of whey fibrils on the pores of the carbonous matrix. Overall, the spectra showed the elemental distributions of carbon (C, 86.6 %), oxygen (O, 6.6 %), nitrogen (N, 5.5 %) and sulphur (S, 1.3 %). In particular, the distribution of N across the material surface was higher than that of S, which could be attributed to the content of nitrogen-rich proteins in whey (β-Lg and α-La) (Moatsou et al., 2003). As such, after WPF binding to AC, an amorphous adsorbent with whey proteins' active elements was obtained, which is desirable for heavy metal adsorption.

The XRD patters of AC, WPF and AC/WPF are reported in Fig. 2. The diffraction pattern of AC exhibited two broad peaks at ~ 23.9° and 43.7°2θ, which were consistent with typical amorphous graphitic planes comprised of aromatic rings and aliphatic chains (Martin et al., 2023). The remaining sharp and strong peaks (20.9°, 26.6°, 36.6°, 39.5°, 50.1° and 54.8°2θ) were identified as quartz (SiO_2) (ICDD No. 00–046-1045), corresponding to their lattice planes (1 0 0), (1 0 1), (1 1 0), (1 0 2), (1 1 2) and (2 0 2), respectively. This non-clay mineral was identified in other studies where this commercial activated carbon was used (Santos et al., 2021; Zhirou Wang & Jang, 2022). In the XRD pattern of WPF, no indexed peaks were found, indicating the amorphous nature of whey. However, two broad peaks located at 8.3 and 19.7 °2θ were related to α-helix and β-sheet structures, respectively, with the latter as the sharpest as whey amyloids consist mainly of a cross-β-structure, where amino acid segments of its protein profile (e.g., β-Lg) are bonded by van der Waals and hydrogen bonds (Vinayagam et al., 2022). The AC/WPF composite also exhibits the crystalline structures ascribed to both the graphitic phase and quartz, but the crystallinity was higher than those of activated carbon alone. This behaviour could be due to an increase in organic matter by whey fibrils assembling onto the carbonous matrix (Shi et al., 2023).

Further, obtained N_2 adsorption–desorption isotherms are depicted in Fig. 3a. According to the International Union of Pure and Applied

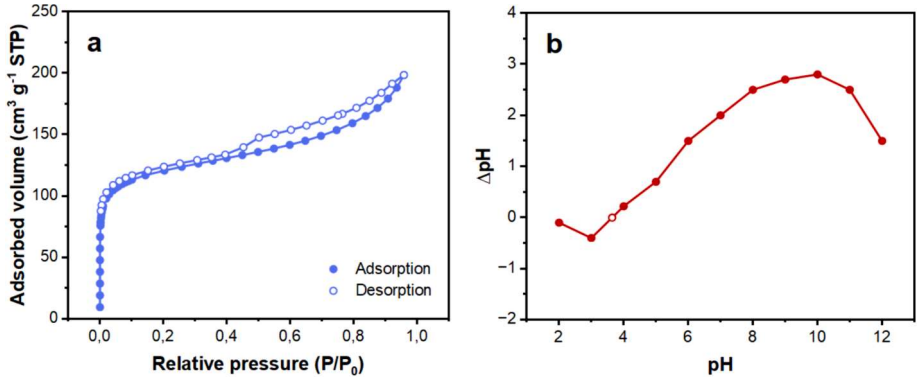

Fig. 3. (a) N_2 adsorption–desorption isotherms and (b) pH at point of zero charge of AC/WPF composite.

Table 1
Textural parameters of AC and AC/WPF samples.

Sample	S_{BET} (m^2/g)	S_{micro} (m^2/g)	S_{ext} (m^2/g)	V_{tot} (cm^3 g^{-1})	Pore width (nm)
AC	900.77	606.48	294.29	0.30	5.85
AC/WPF	455.83	295.92	159.91	0.16	5.91

Chemistry (IUPAC) classification, isotherms correspond to a type IV with an H3 hysteresis loop, characteristic of mesoporous materials with plate-like pores that are commonly used as industrial adsorbents. In this case, monolayer adsorption is accompanied by capillary condensation within pores, which occur for pores wider than 4 nm. The pronounced uptake seen at $P/P_0 < 0.1$ also suggests the presence of micropores in the material (Thommes et al., 2015). Textural parameters of the composite and activated carbon are reported in Table 1. Surface area and total pore volume of AC (S_{BET}: 900.77 m^2/g, V_{tot}: 0.30 cm^3 g^{-1}) decreased to 455.83 m^2/g and 0.16 cm^3 g^{-1}, respectively, due to the incorporation of whey fibrils, confirming successful adhesion of amyloids onto the AC surface. Adsorbent pore size (5.91 nm) corresponds to the pore size range of mesoporous materials and is larger than the diameter of possible arsenic species (~0.8 nm) to be adsorbed (Li et al., 2016).

The pH_{pzc} value of the activated carbon used as precursor is 5.2 and this value dropped to 3.6 after amyloid loading (Fig. 3b), which falls within the reported pH_{pzc} for this composite material (Ramírez-Rodríguez et al., 2020). This means that the surface of AC/WPF will have a net positive charge below pH 3.6, and a net negative surface charge above 3.6. Dissolved inorganic arsenic species depend on pH solution (Fig. S1), and at aqueous pH higher than pH_{pzc} the dominant species are anions, specifically $H_2AsO_4^-$. Thus, it is inferred that electrostatic repulsions will take place between the material surface and arsenic ions, resulting in a decrease in adsorption capacity (Sreeram et al., 2017).

Thermal properties of AC and AC/WPF samples are shown in Fig. 4. The TGA curve for AC consisted of one main region of decomposition: from RT to 100 °C. This stage accounted for a weight loss of 11.17 %, due to residual water evaporation and degradation of highly volatile matter. Then, consistent but minimal reduction in weight can be observed up to 900 °C, which may be attributed to the loss of volatile organic compounds followed by the carbonous content decomposition into ash and CO_2 release (Yanti et al., 2023; Zaidi & Sorokhaibam, 2021). As for the composite, some differences regarding the pure AC are observed. Weight loss rate from the dehydration stage (25–110 °C) was ~ 2 % higher than AC, and a second stage of weight loss appeared (220–480 °C), ascribed to decomposition of whey proteins (Seiwert et al., 2021). This provides further evidence of both precursors in the composite and supports the results of the EDX analysis, which showed the weight percentage of N and S. From the DTG curves (Fig. 4b), maximum thermal degradation temperatures of AC and AC/WPF were 59 and 64 °C, respectively, indicating that the composite maintained the thermal stability of AC despite of having more organic matter on its matrix.

3.2. Adsorption properties of the hybrid composite

3.2.1. Effect of solution pH

Fig. 5 shows the result of batch studies performed to evaluate the impact of solution pH on arsenic removal. As^{5+} would exist as H_3AsO_4 precipitate at pH lower than 5.0 according to its speciation diagram, so AC/WPF was examined at a pH range of 5.0–13.0. Arsenate adsorption decreased with the increase of solution pH, as expected due to the pH at point of zero charge of the material. This can be attributed to the presence of OH– in the media at alkaline pH values and its competitive effect between these anions and arsenate. As the net negative charge of the adsorbent decreased with pH, availability of adsorption sites increased, which in turn generated the highest adsorption capacity at pH 5.0 (Maji et al., 2018). These results confirmed that at working pH there is an electrostatic hindrance on arsenic removal, and could imply that chemical interactions, particularly inner complexation, are the predominant mechanisms of the adsorption process (Merodio-Morales et al., 2020). The same behaviour was noticed for chromium removal, another anion, as reported in a previous study (Ramírez-Rodríguez et al., 2020). It is noteworthy that at the optimum solution pH, activated carbon alone had an adsorption capacity of 0.04 mmol g^{-1}, showing a 35 % decrease in arsenic uptake when comparing it to the hybrid material.

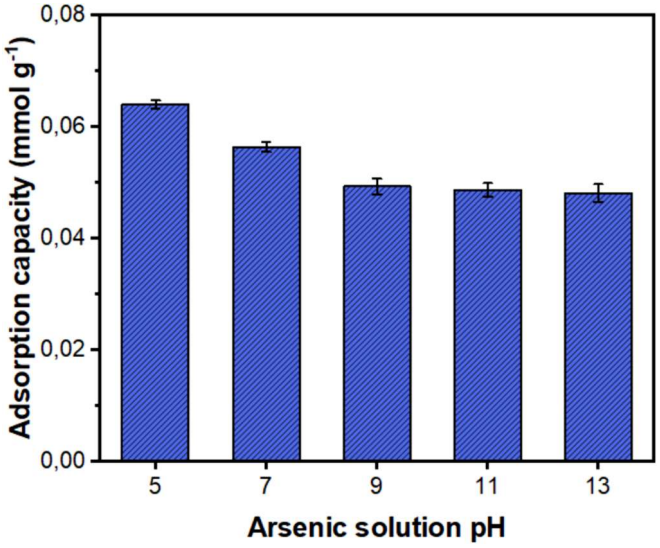

Fig. 5. Effect of solution pH on AC/WPF adsorption capacity for arsenic removal.

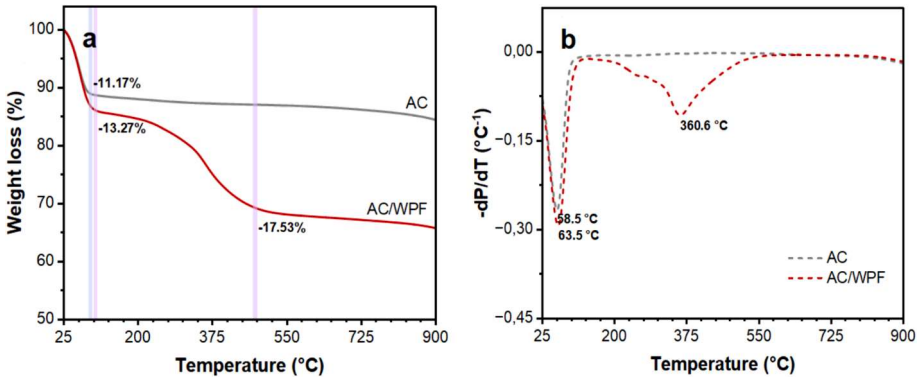

Fig. 4. (a) Thermogravimetric and (b) differential thermic analysis curves of activated carbon (AC) and the hybrid material (AC/WPF).

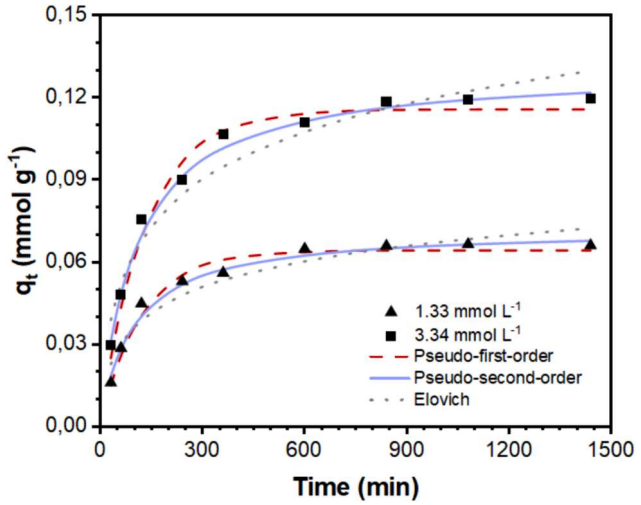

Fig. 6. Kinetic modelling of arsenic adsorption on AC/WPF at 1.33 mmol/L and 3.34 mmol/L (30 °C, pH 5.0).

Table 2
Kinetic parameters estimated for arsenic adsorption on AC/WPF at pH 5.0 and 30 °C.

Model	Parameter	Concentration (mmol L^{-1})	
		1.33	3.34
Pseudo-first order	k_1	0.009	0.0082
	q_e	0.06	0.12
	R^2	0.97	0.98
	SSE	0.06	0.07
	χ^2	0	0
Pseudo-second order	k_2	0.16	0.08
	q_e	0.07	0.13
	R^2	0.99	0.99
	SSE	0.04	0.02
	χ^2	0	0
Elovich	α	0.002	0.0031
	β	74.29	40.14
	R^2	0.94	0.95
	SSE	0.12	0.1
	χ^2	0.01	0.01

3.2.2. Adsorption kinetics

Arsenic adsorption kinetic experiments were used to analyse the rate of adsorbate transfer from the aqueous media to the adsorbent surface, as well as predicting the minimum time needed for the process (Yaoxing Liu et al., 2022). The results of non-linear fitted kinetic models are provided in Fig. 6 and model parameters, as well as their correlation and error analysis metrics, are presented in Table 2. The adsorbed amount of arsenic increased rather rapidly in the first 4 h, followed by a slower rate of adsorption, and then an equilibrium state was attained after 8 h at all tested initial arsenic concentrations. This behaviour may be attributed to a fast initial adsorption on the surface's available active sites and also a high arsenic mass transfer, followed by ions diffusion into the hybrid material's mesopores and micropores and subsequent loading and saturation of functional groups (Xiaotao Zhang et al., 2017). Weak electrostatic interactions predicted in the pH_{pzc} analysis can also contribute to the long equilibrium time (Tan et al., 2020b). After 18 h of contact time, no significant change in adsorption capacity was noticed, meaning the adsorbent surface was fully saturated.

Comparing kinetic models, the pseudo-second-order model was found to provide the best data fitting with $R^2 > 0.99$ and lower values of *SSE* and statistical errors (χ^2) than those obtained for the PFO and Elovich models. Likewise, the calculated adsorption capacity was consistent to the experimental values obtained for 1.33 and 3.34 mmol/L. Therefore, arsenic removal by AC/WPF can be described by the PSO model suggesting a chemisorption process and that interaction of adsorbate and adsorption sites can be expected to be a rate-controlling step in this separation process (Dudek & Kołodyńska, 2022; Kumar et al., 2021). Results are in accordance to those reported for adsorptive materials, as modified porous adsorbents, particularly activated carbons and chars, have abundant functional sites where pollutant kinetics are governed by their availability (J. Wang & Guo, 2020).

Table 3
Parameters of isotherm models for arsenic adsorption at pH 5.0.

Model	Temperature (°C)		
	20	30	40
Langmuir			
q_m	0.31	0.3	0.29
K_L	0.2	0.23	0.26
R^2	0.94	0.97	0.97
SSE	0.26	0.13	0.17
χ^2	0.03	0.01	0.02
Freundlich			
K_F	0.05	0.06	0.06
n	1.43	1.48	1.53
R^2	0.9	0.94	0.92
SSE	0.32	0.2	0.24
χ^2	0.04	0.02	0.03
Sips			
q_m	0.16	0.17	0.18
K_S	0.6	0.58	0.61
β_S	2.01	1.75	1.72
R^2	0.98	0.98	0.99
SSE	0.09	0.11	0.05
χ^2	0.01	0.01	0
Dubinin-Radushkevich			
q_S	0.15	0.15	0.15
K_{DR}	0.0014	0.0011	0.0009
R^2	0.95	0.96	0.92
SSE	0.24	0.22	0.25
χ^2	0.02	0.02	0.03

3.2.3. Adsorption equilibrium and thermodynamics

Adsorption isotherms relate the adsorbate accumulation into the adsorbent surface at constant temperature, as well as depicting the adsorption saturation of the material, its nature and interaction type (Akdemir et al., 2022). Fitting results of arsenic adsorption on AC/WPF at different temperatures (20–40 °C) and pH 5.0 are summarized in Table 3, while a comparison of the non-linear regression analysis done with all models is presented in Fig. 7a-c. Sips model provided the best estimate of the experimental data showing high determination coefficients ($R^2 > 0.98$) and low error analysis metrics (*SSE* < 0.11 and $\chi^2 < 0.01$). Hereby, the maximum adsorption capacity obtained was 0.14 mmol g^{-1}, 0.15 mmol g^{-1} and 0.16 mmol g^{-1} for 20, 30 and 40 °C, respectively. These values were compared with analogous carbonous adsorbents, including biomass-derived activated carbons and biochars (BC), (Table 4), proving that AC/WPF has a similar performance for As^{5+} removal despite of its relative low surface area in comparison with other materials. Therefore, the present composite can be considered as a low-cost alternative for advanced treatment of arsenic-bearing effluents, especially seeing as it procures less processed raw materials by repurposing whey.

According to the Sips model, the adsorption mechanism of arsenic on AC/WPF is a combination of diffusion at low solute concentrations and monolayer formation at high solute concentrations (Zhuo Wang et al., 2022). Nevertheless, other model parameters provide useful insight regarding the adsorption process. For instance, Freundlich constants (1.43–1.53) were within the range $1 < n < 10$, which indicated a thermodynamically feasible adsorption. This model, however, showed lower determination coefficients and higher predicted errors than those of Langmuir modelling data in the studied temperatures range, suggesting that arsenate adsorption occurred mainly at energetically homogenous active sites of the composite, with an equal affinity towards arsenic ions,

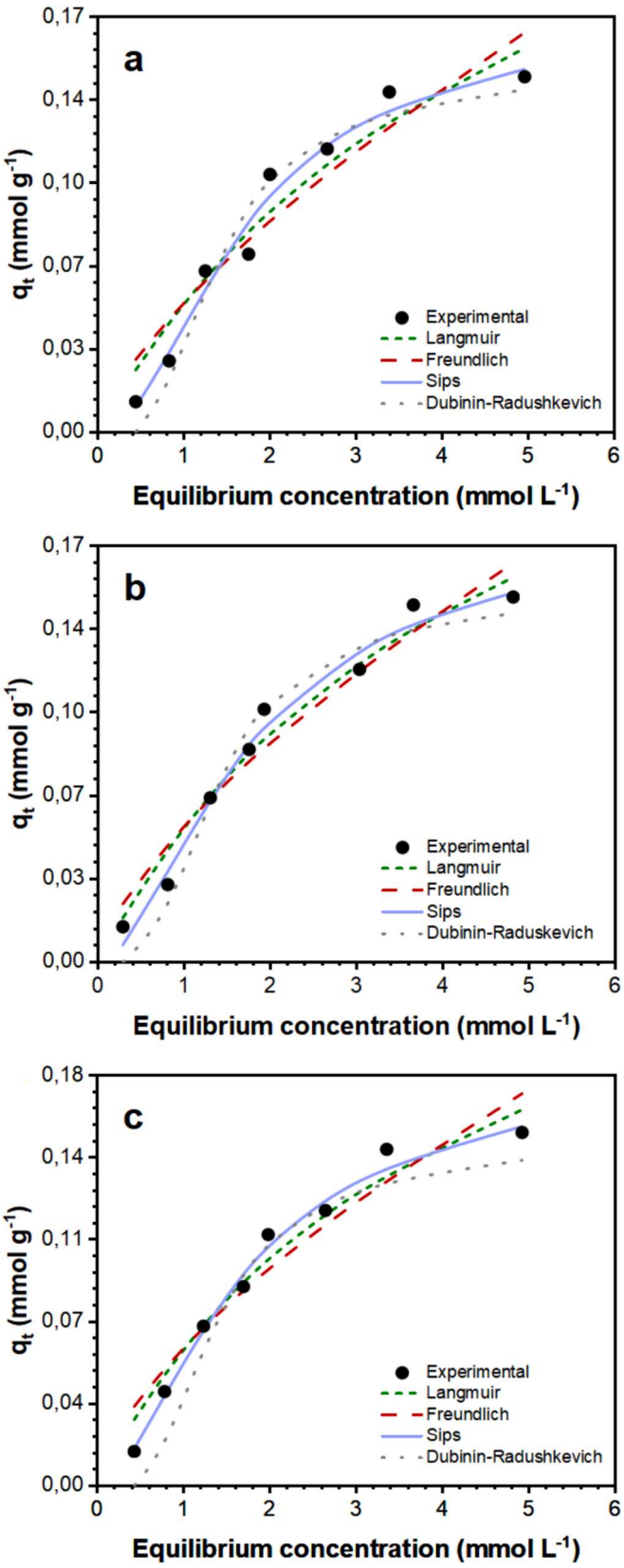

Fig. 7. Isotherm modelling of arsenic adsorption on AC/WPF at pH 5.0 and (a) 20 °C, (b) 30 °C and (c) 40 °C.

Table 4
Results reported of the application of carbon-based adsorbents for arsenic removal from water.

Adsorbent	S_{BET} (m^2/g)	Adsorption conditions			q_m (mmol/g)	Ref.
		pH	T (°C)	AD (g/L)		
Fe_2O_3-AC fibres	842.0	7	25	0.5	0.19	(Chen et al., 2016)
Magnetic BC	115.4	6	25	0.8	0.09	(Tan et al., 2020a)
Bamboo AC	1855.0	7	25	1	0.21	(Gao et al., 2023)
Zn lignin BC	255.0	6	–	1	0.26	(Park et al., 2021)
Fe_2O_3 bentonite-AC	433.0	4.5	25	2	0.07	(Pawar et al., 2018)
La avocado seeds BC	29.0	7	25	2	0.20	(Merodio-Morales et al., 2022)
Al-Zn canola straw BC	215	–	25	1	0.16	(Zoroufchi Benis et al., 2022)
AC/WPF	455.8	5	30	4	0.15	This work

which is characteristic of monolayer adsorption (Al-Ghouti and Da'ana, 2020).

On the other hand, the Dubinin-Radushkevich isotherm was used to determine whether the adsorption process is physical or chemical, according to the adsorption energy of AC/WPF (Eq. (2).

$$E = (2K_{DR})^{-0.5} \quad (2)$$

Literature indicates that the adsorption occurs physically if the value of E is lower than 8 kJ mol^{-1}, whereas chemical adsorption occurs if the E is greater than 16 kJ mol^{-1}. Ion exchange occurs when E values are between 8 and 16 kJ mol^{-1} (Akdemir et al., 2022). Adsorption energies calculated for arsenic removal were 19.2, 20.9 and 23.0 kJ mol^{-1} at 20, 30 and 40 °C, respectively. Therefore, the results show that the adsorption mechanism of AC/WPF is mainly linked to chemical forces, confirming the removal mechanism implied in section 3.2.2. Overall, the determination coefficients and error analysis metrics indicated that the isotherm models obeyed the following trend in terms of their applicability: Sips > Langmuir > Dubinin-Radushkevich > Freundlich. All adsorption isotherms were classed as classical L2-type isotherms according to Giles' isotherm classification (Giles et al., 1960). Moreover, they showed that the adsorption capacity increased with the increase of temperature, suggesting an endothermic process. This claim was confirmed via the estimation of standard enthalpy ($\Delta H°$, kJ mol^{-1}) according to the van't Hoff approach. The calculated enthalpy for As^{5+} adsorption onto AC/WPF was 46.73 kJ mol^{-1}, thus indicating an endothermic adsorption process, which supports the behaviour seen in Fig. 7. This enthalpy value lies within the range of both physical and chemical interactions, with the formation of metallic complexes as the main factor behind arsenate removal (Yu Liu & Liu, 2008).

3.2.4. *Effect of interfering ions*

Given that industrial wastewater and mining runoffs are complex matrices of various chemical species, including heavy, alkali and alkaline earth metals, the adsorption capacity of AC/WPF composite for As^{5+} was assessed in a media containing lead (Pb^{2+}), and both calcium (Ca^{2+}) and sodium (Na^{+}) ions, respectively. It was found that the arsenic adsorption capacity increased significantly ($p = 0.01$) up to 0.04 mmol g^{-1} by increasing the initial Pb^{2+} concentration from 0.7 to 1.3 mmol/L, while no significant difference ($p = 0.23$) in adsorption was observed when arsenate co-existed with the same range of concentrations of Ca^{2+}

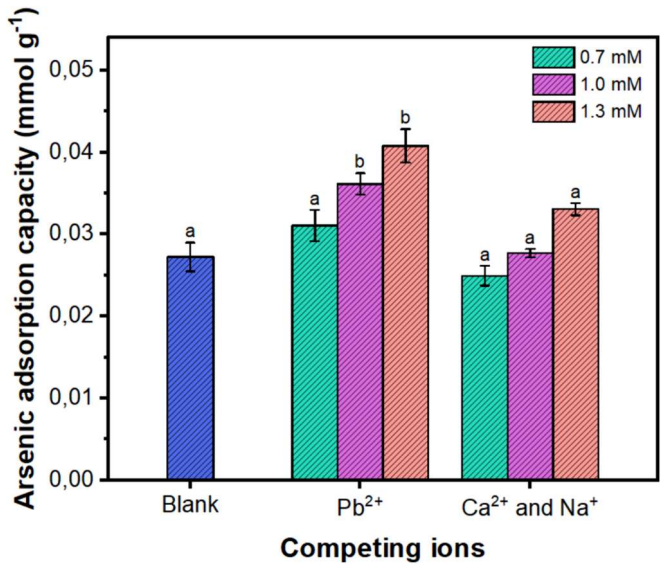

Fig. 8. Effect of co-existing metal ions on adsorption of arsenic of AC/WPF (30 °C, pH 5.0, C_0 = 0.67 mmol/L). Error bars represent standard deviations with n = 3. Different letters indicate significant difference ($p < 0.05$) between samples.

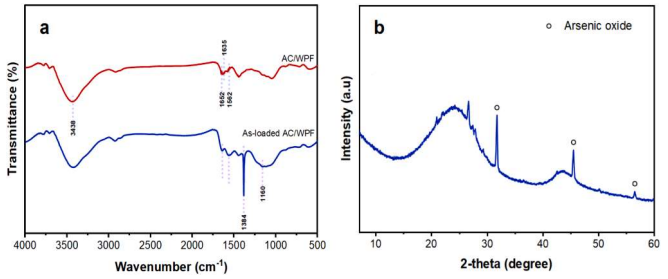

Fig. 9. (a) FT-IR spectra and (b) X-ray diffraction pattern of AC/WPF used for arsenic adsorption (30 °C, pH 5.0, C_0 = 5.34 mmol/L).

and Na^+. In general, the trend seen in Fig. 8 may be attributed to the higher amount of cations in the adsorbate solution, which promoted the protonation of the material and favoured the binding of arsenic by electrostatic interactions (Wei et al., 2022). The difference of remarked contaminant uptake between the As-Pb and the As-Ca-Na systems, can be related to the electronegativity order between interfering ions (Pb^{2+} > Ca^{2+} > Na^+), meaning a stronger affinity between lead and the functional groups of AC/WPF (Fosso-Kankeu et al., 2011), and the promotion of chemical complexes and electrostatic attraction between lead and arsenate, as demonstrated by Vaca-Escobar et al. (2012). Nevertheless, as the adsorbent is not susceptible to ionic strength (light metals concentration), its adsorption mechanism is governed by ligand exchange, which is evidence of the importance of chemisorption in the removal of arsenic (Yin et al., 2021). Overall, these results suggest that AC/WPF is a promising adsorbent that could be applied for treatment of real arsenic contaminated water sources.

3.2.5. *Mechanism of adsorption process*

To clarify the adsorption mechanism of As^{5+} on AC/WPF, FT-IR and XRD analyses were performed to identify the surface changes after arsenic loading. For the case of FT-IR spectra (Fig. 9a), secondary structures of whey proteins can be identified in the fresh composite through the primary amide region (1700–1600 cm^{-1}) via the C = O carbonyl stretch, where the absorption bands at 1652 and 1625 cm^{-1} are assigned to α-helix and β-sheet structures, respectively (Han et al., 2022). Also, the absorption band representing bending vibrations of

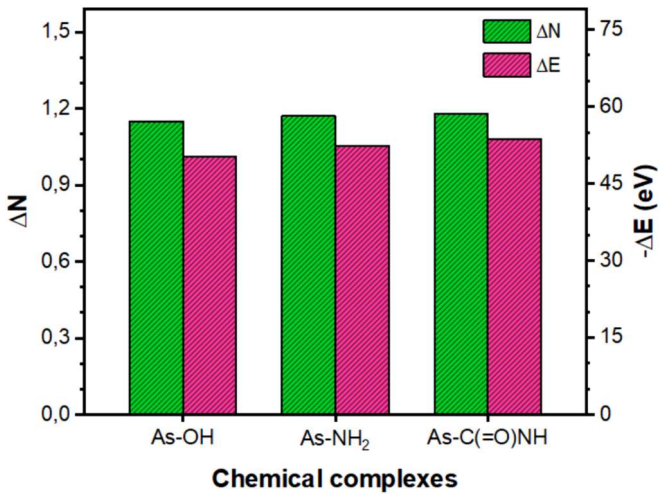

Fig. 10. Charge transfer (ΔN) and energy lowering (ΔE) induced by As^{5+} adsorption.

secondary amide groups appeared at 1562 cm^{-1}, while the absorption band found at 3438 cm^{-1} corresponds to stretching vibrations of primary amino groups and hydrogen bonds (Ramírez-Rodríguez et al., 2020). After arsenate adsorption, this broad signal was reduced, suggesting that O-H functional groups participate on arsenic binding to the adsorbent. On the contrary case, amide bands corresponding to β-sheets and amide II increased considerably their intensity, the α-helix absorption band disappeared and a new well-defined absorption band appeared at 1384 cm^{-1}, which can be attributed to As-O bond (Merodio-Morales et al., 2022; Park et al., 2021). Therefore, arsenic adsorption changed the protein fraction organization of the composite to a higher content of β-sheets, which has been reported in other studies regarding whey fibrils adsorption properties (C. Zhang et al., 2021). These results are supported by the changes observed in the crystalline structure of the arsenate-loaded adsorbent (Fig. 9b); new diffraction peaks (31.7, 45.5 and 56.5 °2θ) were identified as arsenic oxide (As_2O_3) (ICDD No. 01–084-7622). Moreover, the increase of intensity of the broad peak at 24.2° confirmed the change of protein structure.

The adsorption affinity between arsenic and the hydroxyl, amide, and amino functional groups can be further identified via the HSAB principle, wherein heavy metals and adsorption sites are treated as Lewis acids, or electron acceptors, and Lewis bases, or electron donors, respectively (Bulin, 2023). The chemical reactivity of an adsorbate-adsorbent system can be characterized by the number of electrons transferred between them (electron transfer, ΔN) and the resistance to change of the chemical potential (energy lowering, ΔE), which were determined using the following equations (Eqs. (3) and (4) (Bulin et al., 2022):

$$\Delta N = \frac{X_A - X_B}{2(\eta_A + \eta_B)} \tag{3}$$

$$\Delta E = -\frac{(X_A - X_B)^2}{4(\eta_A + \eta_B)} \tag{4}$$

Where X_A and X_B are the absolute electronegativity of acid and base (eV), respectively, while η_A and η_B refer to the correspondent absolute hardness (eV). The related parameters of As, OH, NH_2 and C(=O)NH, are reported in Table S3, with their respective calculated values of ΔN and ΔE depicted in Fig. 10. Herein, the high energy lowering of each interaction exemplifies the binding affinity between the functional groups of AC/WPF as hard bases and arsenic as a hard acid, behaviour predicted by the HSAB theory (Pearson, 1988; Tang et al., 2022). Thus, the chemical complexes formed followed the subsequent order according to their strength: C(=O)NH > NH_2 > OH. These findings, coupled with the

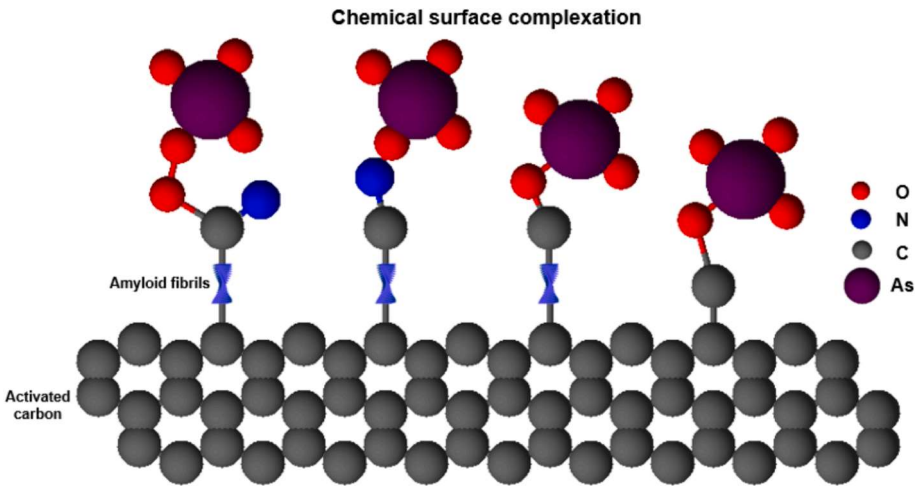

Fig. 11. Proposed adsorption mechanism for the removal of As^{5+} with AC/WPF.

surface characterization of the material after adsorption, lead to the proposed adsorption mechanism for As^{5+} on AC/WPF composite, portrayed in Fig. 11.

3.3. Economic analysis

The economic viability of an adsorbent is an important factor to estimate its application potential as a wastewater treatment for non-conventional pollutants like heavy metals. The cost analysis of the hybrid composite was assessed by considering the adsorption cost (USD) associated with the removal of 1 mmol of adsorbate, in this case arsenate, calculated according to an equation modified from Ighalo et al. (2022) (Eq. (5):

$$Adsorption\ cost = \frac{C_{RM} + C_U}{q_m} \quad (5)$$

Where C_{RM} and C_U are the cost of raw materials and utilities (USD g_{ads}^{-1}), respectively, while q_m is the maximum arsenic adsorption capacity, taken at 30 °C (mmol g^{-1}). The related expenses of AC/WPF production is presented in Table S4; total production cost was \$1.7 $mmol^{-1}$. Compared to DARCO activated carbon (\$3.5 $mmol^{-1}$), evaluated in this study, and modified peanut shell biochar (\$1.4 $mmol^{-1}$) (Kushwaha et al., 2023), the adsorbent cost of AC/WPF is competitive economically and illustrates the viability of using whey protein amyloid fibrils for a potential application as commercially available adsorbents. This adsorption cost could be further reduced using a biomass-derived activated carbon, as it was observed that almost 50 % of the total cost was due to the use of DARCO activated carbon. However, for a better estimation of the performance and cost involved of AC/WPF composite, pilot scale cost assessment via CAPEX and OPEX should be carried out.

4. Conclusions

In this study, a novel adsorbent AC/WPF was successfully prepared by material doping combined with vacuum filtration method. This adsorptive membrane exhibited good specific surface area, porous structure, and prominent functional groups (amide and amine groups from whey proteins and hydroxyl groups of activated carbon) to capture inorganic pollutants such as arsenate. The material showed efficient capacity for removing As^{5+} in an aqueous phase at optimized pH, even in the presence of interfering metals. The adsorption data fitted well to the Sips isotherm, with a maximum arsenate adsorption capacity of 0.14–0.16 mmol g^{-1} at 20–40 °C. The adsorption process followed PSO kinetics, which suggested that arsenate ions adhered to the material surface by chemisorption. The adsorption mechanism entailed the formation of As-O bond via electron donation between whey fibrils' groups and arsenate ion, showing the adsorption capacity and application of this nanostructures. Considering all the results, the proposed hybrid material is an inexpensive and effective adsorbent to remove arsenic from water and holds great promise for a potential use in wastewater remediation of this contaminant, especially regarding mining derived run-offs.

CRediT authorship contribution statement

Mateo Andrés Gallardo Salas: Writing – original draft, Methodology, Investigation, Formal analysis, Conceptualization. **Didilia Ileana Mendoza-Castillo:** Writing – review & editing, Investigation, Formal analysis. **Adrián Bonilla-Petriciolet:** Writing – review & editing, Supervision. **Carlos Jiménez-Junca:** Writing – review & editing, Supervision, Project administration.

Declaration of competing interest

The authors declare that they have no known competing financial interests or personal relationships that could have appeared to influence the work reported in this paper.

Data availability

Data will be made available on request.

Acknowledgements

The authors would like to thank Universidad de La Sabana for the financial support provided (Project code ING-287-2021). Mateo Andres Gallardo Salas would like to personally acknowledge the Chemical Engineering Department of Instituto Tecnológico de Aguascalientes for their support in the development of this article and Universidad de La Sabana for the scholarship for his master's studies.

Appendix A. Supplementary data

Supplementary data to this article can be found online at https://doi.org/10.1016/j.enmm.2024.100956.

References

Akdemir, M., Isik, B., Cakar, F., Cankurtaran, O., 2022. Comparison of the adsorption efficiency of cationic (Crystal Violet) and anionic (Congo Red) dyes on Valeriana officinalis roots: Isotherms, kinetics, thermodynamic studies, and error functions.

Mater. Chem. Phys. 291, 126763 https://doi.org/10.1016/j.matchemphys.2022.126763.
Al-Ghouti, M.A., Da'ana, D.A., 2020. Guidelines for the use and interpretation of adsorption isotherm models: A review. J. Hazard. Mater. 393, 122383 https://doi.org/10.1016/j.jhazmat.2020.122383.
Azam, M.R., Tan, I.M., Ismail, L., Mushtaq, M., Nadeem, M., Sagir, M., 2013. Static adsorption of anionic surfactant onto crushed Berea sandstone. J. Pet. Explor. Prod. Technol. 3, 195–201. https://doi.org/10.1007/s13202-013-0057-y.
Bi, J., Tao, Q., Huang, X., Wang, J., Wang, T., Hao, H., 2021. Simultaneous decontamination of multi-pollutants: A promising approach for water remediation. Chemosphere 284, 131270. https://doi.org/10.1016/J.CHEMOSPHERE.2021.131270.
Bolisetty, S., Mezzenga, R., 2016. Amyloid-carbon hybrid membranes for universal water purification. Nat. Nanotechnol. 11, 365–371. https://doi.org/10.1038/nnano.2015.310.
Bucatariu, F., Ghiorghita, C.-A., Schwarz, D., Boita, T., Mihai, M., 2019. Layer-by-layer polyelectrolyte architectures with ultra-fast and high loading/release properties for copper ions. Colloids Surfaces A: Physicoch. Eng. Aspects 579, 123704. https://doi.org/10.1016/j.colsurfa.2019.123704.
Bulin, C., 2023. Adsorption mechanism and removal efficiency of magnetic graphene oxide-chitosan hybrid on aqueous Zn(II). Int. J. Biol. Macromol. 241, 124588 https://doi.org/10.1016/j.ijbiomac.2023.124588.
Bulin, C., Zheng, R., Guo, T., Zhang, B., 2022. Incorporating hard-soft acid-base theory in multi-aspect analysis of the adsorption mechanism of aqueous heavy metals by graphene oxide. J. Phys. Chem. Solid 170, 110934. https://doi.org/10.1016/j.jpcs.2022.110934.
Bundschuh, J., Armienta, M.A., Morales-Simfors, N., Alam, M.A., López, D.L., Delgado Quezada, V., Dietrich, S., Schneider, J., Tapia, J., Sracek, O., Castillo, E., Parra, L.-M.-M., Altamirano Espinoza, M., Guimarães Guilherme, L.R., Sosa, N.N., Niazi, N.K., Tomaszewska, B., Lizama Allende, K., Bieger, K., Ahmad, A., 2021. Arsenic in Latin America: New findings on source, mobilization and mobility in human environments in 20 countries based on decadal research 2010–2020. Crit. Rev. Environ. Sci. Technol. 51 (16), 1727–1865. https://doi.org/10.1080/10643389.2020.1770527.
Chen, H., Lv, K., Du, Y., Ye, H., Du, D., 2016. Microwave-assisted rapid synthesis of Fe2O3/ACF hybrid for high efficient As(V) removal. J. Alloy. Compd. 674, 399–405. https://doi.org/10.1016/j.jallcom.2016.03.024.
Ciopec, M., Biliuta, G., Negrea, A., Duțeanu, N., Coseri, S., Negrea, P., Ghangrekar, M., 2021. Testing of chemically activated cellulose fibers as adsorbents for treatment of arsenic contaminated water. Materials 14 (3731), 1–20. https://doi.org/10.3390/ma14133731.
De Oliveira, E.C.M., Pires, L.P., Santos, V.S.V., Caixeta, E.S., Bravo, J.V.M., Pereira, B.B., 2023. Phytoremediation, bioaccessibility and ecotoxicological risk assessment of arsenic in a gold mining area. Chemosphere 319, 138030. https://doi.org/10.1016/j.chemosphere.2023.138030.
Dudek, S., Kołodyńska, D., 2022. Arsenic(V) removal on the lanthanum-modified ion exchanger with quaternary ammonium groups based on iron oxide. J. Mol. Liq. 347, 117985 https://doi.org/10.1016/j.molliq.2021.117985.
Emo, B., Eberlin, C.T., Hixon, K.R., Growney Kalaf, E.A., Laktas, J.M., Sell, S.A., 2017. A study on the potential of doped electrospun polystyrene fibers in arsenic filtration. J. Environ. Chem. Eng. 5, 232–239. https://doi.org/10.1016/j.jece.2016.11.039.
Fan, Y., Lan, H., Qi, Z., Liu, R., Hu, C., 2022. Removal of nickel and copper ions in strongly acidic conditions by in-situ formed amyloid fibrils. Chemosphere 297, 134241. https://doi.org/10.1016/j.chemosphere.2022.134241.
Fontana, K.B., Lenzi, G.G., Seára, E.C.R., Chaves, E.S., 2018. Comparision of photocatalysis and photolysis processes for arsenic oxidation in water. Ecotoxicol. Environ. Saf. 151, 127–131. https://doi.org/10.1016/j.ecoenv.2018.01.001.
Fosso-Kankeu, E., Mulaba-Bafubiandi, A.F., Mamba, B.B., Barnard, T.G., 2011. Prediction of metal-adsorption behaviour in the remediation of water contamination using indigenous microorganisms. J. Environ. Manage. 92 (10), 2786–2793. https://doi.org/10.1016/J.JENVMAN.2011.06.025.
Gao, Q., Feng, Z., He, Y., Hou, Y., Ren, H., Su, M., Ni, L., Liu, Z., 2023. Pyrolysis self-activation: An environmentally friendly method to transform biowaste into activated carbon for arsenic removal. Bioresour. Technol. 368, 128353 https://doi.org/10.1016/j.biortech.2022.128353.
Giles, C.H., MacEwan, T.H., Nakhwa, S.N., Smith, D., 1960. Studies in Adsorption. Part XI. A system system of classification of solution adsorption isotherms, and its use in diagnosis of adsorption mechanisms and in measurement of specific surface areas of solids. J. Chem. Soc. 846, 3973–3993.
Haidar, Z., Fatema, K., Shoily, S.S., Sajib, A.A., 2023. Disease-associated metabolic pathways affected by heavy metals and metalloid. Toxicol. Rep. 10, 554–570. https://doi.org/10.1016/j.toxrep.2023.04.010.
Han, X., Liang, Z., Tian, S., Liu, L., Wang, S., 2022. Epigallocatechin gallate (EGCG) modification of structural and functional properties of whey protein isolate. Food Res. Int. 158, 111534 https://doi.org/10.1016/j.foodres.2022.111534.
Hassan, M.N., Nabi, F., Khan, A.N., Hussain, M., Siddiqui, W.A., Uversky, V.N., Khan, R. H., 2022. The amyloid state of proteins: A boon or bane? Int. J. Biol. Macromol. 200, 593–617. https://doi.org/10.1016/j.ijbiomac.2022.01.115.
Horne, J.D., Brikowski, T.H., Johannesson, K.H., 2023. Natural arsenic-rich spring waters discharging from the Austin Chalk, North-Central Texas, USA: Mineral and chemical evidence of pyrite oxidation followed by reductive dissolution of neo-formed Fe(III) oxides/oxyhydroxides. Appl. Geochem. 150, 105547 https://doi.org/10.1016/j.apgeochem.2022.105547.
Ighalo, J.O., Omoarukhe, F.O., Ojukwu, V.E., Iwuozor, K.O., Igwegbe, C.A., 2022. Cost of adsorbent preparation and usage in wastewater treatment: A review. Cleaner Chemical Engineering 3, 100042. https://doi.org/10.1016/j.clce.2022.100042.
Isabel San-Martín, M., Alonso, R.M., Ivars-Barceló, F., Escapa, A., Morán, A., 2023. Complete arsenic removal from water using biocatalytic systems based on anaerobic films grown on carbon fibers. Catal. Today 423, 114269. https://doi.org/10.1016/j.cattod.2023.114269.
Khalesi, H., Sun, C., He, J., Lu, W., Fang, Y., 2021. The role of amyloid fibrils in the modification of whey protein isolate gels with the form of stranded and particulate microstructures. Food Res. Int. 140, 109856 https://doi.org/10.1016/J.FOODRES.2020.109856.
Kumar, J.A., Kumar, P.S., Krithiga, T., Prabu, D., Amarnath, D.J., Sathish, S., Venkatesan, D., Hosseini-Bandegharaei, A., Prashant, P., 2021. Acenaphthene adsorption onto ultrasonic assisted fatty acid mediated porous activated carbon-characterization, isotherm and kinetic studies. Chemosphere 284, 131249. https://doi.org/10.1016/j.chemosphere.2021.131249.
Kushwaha, R., Singh, R.S., Mohan, D., 2023. Comparative study for sorption of arsenic on peanut shell biochar and modified peanut shell biochar. Bioresour. Technol. 375, 128831 https://doi.org/10.1016/j.biortech.2023.128831.
Lappa, I.K., Papadaki, A., Kachrimanidou, V., Terpou, A., Koulougliotis, D., Eriotou, E., Kopsahelis, N., 2019. Cheese Whey Processing: Integrated Biorefinery Concepts and Emerging Food Applications. Foods 8, 347. https://doi.org/10.3390/foods8080347.
Li, W., Chen, D., Xia, F., Tan, J.Z.Y., Huang, P.-P., Song, W.-G., Nursam, N.M., Caruso, R. A., 2016. Extremely high arsenic removal capacity for mesoporous aluminium magnesium oxide composites. Environ. Sci. Nano 3, 94–106. https://doi.org/10.1039/c5en00171d.
Liu, Y., Dai, L., Ke, X., Ding, J., Wu, X., Chen, R., Ding, R., Van der Bruggen, B., 2022. Arsenic and cation metal removal from copper slag using a bipolar membrane electrodialysis system. J. Clean. Prod. 338, 130662 https://doi.org/10.1016/j.jclepro.2022.130662.
Liu, Yu., Liu, Y.J., 2008. Biosorption isotherms, kinetics and thermodynamics. Sep. Purif. Technol. 61, 229–242. https://doi.org/10.1016/j.seppur.2007.10.002.
Lopes, A. C. A., Eda, S. H., Andrade, R. P., Amorim, J. C., & Duarte, W. F. (2019). New Alcoholic Fermented Beverages—Potentials and Challenges. In *Fermented Beverages: Volume 5. The Science of Beverages* (pp. 577–603). Woodhead Publishing. https://doi.org/10.1016/B978-0-12-815271-3.00014-2.
Lutter, L., Aubrey, L.D., Xue, W.-F., 2021. On the Structural Diversity and Individuality of Polymorphic Amyloid Protein Assemblies. J. Mol. Biol. 433, 167124 https://doi.org/10.1016/J.JMB.2021.167124.
Maji, S., Ghosh, A., Gupta, K., Ghosh, A., Ghorai, U., Santra, A., Sasikumar, P., Ghosh, U. C., 2018. Efficiency evaluation of arsenic(III) adsorption of novel graphene oxide@iron-aluminium oxide composite for the contaminated water purification. Sep. Purif. Technol. 197, 388–400. https://doi.org/10.1016/j.seppur.2018.01.021.
Mariana, M., H.P.S., A. K., Mistar, E. M., Yahya, E. B., Alfatah, T., Danish, M., & Amayreh, M. (2021). Recent advances in activated carbon modification techniques for enhanced heavy metal adsorption. *Journal of Water Process Engineering*, *43*, 102221. https://doi.org/10.1016/J.JWPE.2021.102221.
Marrugo-Negrete, J., Pinedo-Hernández, J., Marrugo-Madrid, S., Paternina-Uribe, R., Ruiz-Fernández, A.C., Sanchez-Cabeza, J.A., 2023. Vertical distribution and trace element contamination in sediment cores affected by gold mining in Colombia. Chemosphere 340, 139744. https://doi.org/10.1016/j.chemosphere.2023.139744.
Martin, G.D., Lara, B., Bounoukta, C.E., Domínguez, M.I., Ammari, F., Ivanova, S., Centeno, M.Á., 2023. Glucose dehydration reaction over metal halides supported on activated charcoal catalysts. Catal. Today 423, 114012. https://doi.org/10.1016/j.cattod.2023.01.019.
Mendoza-Castillo, D.I., Reynel-Ávila, H.E., Bonilla-Petriciolet, A., Silvestre-Albero, J., 2016. Synthesis of denim waste-based adsorbents and their application in water defluoridation. J. Mol. Liq. 221, 469–478. https://doi.org/10.1016/j.molliq.2016.06.005.
Merodio-Morales, E.E., Reynel-Ávila, H.E., Mendoza-Castillo, D.I., Duran-Valle, C.J., Bonilla-Petriciolet, A., 2020. Lanthanum- and cerium-based functionalization of chars and activated carbons for the adsorption of fluoride and arsenic ions. Int. J. Environ. Sci. Technol. 17, 115–128. https://doi.org/10.1007/s13762-019-02437-w.
Merodio-Morales, E.E., Mendoza-Castillo, D.I., Bonilla-Petriciolet, A., Reynel-Avila, H.E., Milella, A., di Bitonto, L., Pastore, C., 2022. A novel CO2 activation at room temperature to prepare an engineered lanthanum-based adsorbent for a sustainable arsenic removal from water. Chem. Eng. Res. Des. 185, 239–252. https://doi.org/10.1016/j.cherd.2022.07.003.
Mladin, G., Ciopec, M., Negrea, A., Duteanu, N., Negrea, P., Ianasi, P., Ianași, C., 2022. Silica- Iron Oxide Nanocomposite Enhanced with Porogen Agent Used for Arsenic Removal. Materials 15, 5366. https://doi.org/10.3390/ma15155366.
Moatsou, G., Hatzinaki, A., Kandarakis, I., Anifantakis, E., 2003. Nitrogenous fractions during the manufacture of whey protein concentrates from Feta cheese whey. Food Chem. 81 (2), 209–217. https://doi.org/10.1016/S0308-8146(02)00414-4.
Mollea, C., Marmo, L., & Bosco, F. (2013). Valorisation of Cheese Whey, a By-Product from the Dairy Industry. In *Food Industry* (pp. 549–588). https://doi.org/10.5772/53159.
Moreira, V.R., Lebron, Y.A.R., Santos, L.V.S., Coutinho de Paula, E., Amaral, M.C.S., 2021. Arsenic contamination, effects and remediation techniques: A special look onto membrane separation processes. Process Saf. Environ. Prot. 148, 604–623. https://doi.org/10.1016/J.PSEP.2020.11.033.
Ouyang, K., Xie, H., Wang, Y., Woo, M.W., Chen, Q., Lai, S., Xiong, H., Zhao, Q., 2023. Whey protein isolate nanofibrils formed with phosphoric acid: Formation, structural characteristics, and emulsion stability. Food Hydrocoll. 135, 108170 https://doi.org/10.1016/j.foodhyd.2022.108170.
Park, J.-H., Lee, J.-H., Lee, S.-L., Hwang, S.-W., Seo, D.-C., 2021. Adsorption behavior of arsenic onto lignin-based biochar decorated with zinc. Colloids and Surfaces a: Physicochemical and Engineering Aspects 626, 127095. https://doi.org/10.1016/j.colsurfa.2021.127095.

Pawar, R.R., Lalhmunsiama, K.M., Kim, J.-G., Hong, S.-M., Sawant, S.Y., Lee, S.M., 2018. Efficient removal of hazardous lead, cadmium, and arsenic from aqueous environment by iron oxide modified clay-activated carbon composite beads. Appl. Clay Sci. 162, 339–350. https://doi.org/10.1016/J.CLAY.2018.06.014.

Pearson, R.G., 1988. Absolute Electronegativity and Hardness: Application to Inorganic Chemistry. Inorg. Chem. 27 (4), 734–740. https://doi.org/10.1021/ic00277a030.

Peydayesh, M., Mezzenga, R., 2021. Protein nanofibrils for next generation sustainable water purification. Nat. Commun. 12, 1–17. https://doi.org/10.1038/s41467-021-23388-2.

Ramírez-Rodríguez, L.C., Díaz Barrera, L.E., Quintanilla-Carvajal, M.X., Mendoza-Castillo, D.I., Bonilla-Petriciolet, A., Jiménez-Junca, C., 2020. Preparation of a Hybrid Membrane from Whey Protein Fibrils and Activated Carbon to Remove Mercury and Chromium from Water. Membranes 10, 386. https://doi.org/10.3390/membranes10120386.

Saghir, S., Pu, C., Fu, E., Wang, Y., Xiao, Z., 2022. Synthesis of high surface area porous biochar obtained from pistachio shells for the efficient adsorption of organic dyes from polluted water. Surf. Interfaces 34, 102357. https://doi.org/10.1016/j.surfin.2022.102357.

Salazar-Camacho, C., Salas-Moreno, M., Marrugo-Madrid, S., Paternina-Uribe, R., Marrugo-Negrete, J., Díez, S., 2022. A human health risk assessment of methylmercury, arsenic and metals in a tropical river basin impacted by gold mining in the Colombian Pacific region. Environ. Res. 212, 113120 https://doi.org/10.1016/j.envres.2022.113120.

Santos, J.L., Megías-Sayago, C., Ivanova, S., Centeno, M.Á., Odriozola, J.A., 2021. Structure-sensitivity of formic acid dehydrogenation reaction over additive-free Pd NPs supported on activated carbon. Chem. Eng. J. 420 (October 2020) https://doi.org/10.1016/j.cej.2020.127641.

Seiwert, K., Kamdem, D.-P., Kocabaş, D.S., Ustunol, Z., 2021. Development and characterization of whey protein isolate and xylan composite films with and without enzymatic crosslinking. Food Hydrocoll. 120, 106847 https://doi.org/10.1016/j.foodhyd.2021.106847.

Shaji, E., Santosh, M., Sarath, K.V., Prakash, P., Deepchand, V., Divya, B.V., 2021. Arsenic contamination of groundwater: A global synopsis with focus on the Indian Peninsula. Geosci. Front. 12, 101079 https://doi.org/10.1016/J.GSF.2020.08.015.

Sharma, A., Kesamsetty, D., Debnath, J., Ghosh, K.S., 2023. Inhibition of lysozyme amyloid fibrillation by curcumin-conjugated silver nanoparticles: A multispectroscopic molecular level study. J. Mol. Liq. 372, 121156 https://doi.org/10.1016/j.molliq.2022.121156.

Shi, G., Shi, C., Luo, Y., Hong, H., Zhang, J., Li, Y., Tan, Y., 2023. Interaction and phase behavior of whey protein and propylene glycol alginate complex condensates. Food Chem. 404, 134556 https://doi.org/10.1016/j.foodchem.2022.134556.

Soon, W.L., Peydayesh, M., Mezzenga, R., Miserez, A., 2022. Plant-based amyloids from food waste for removal of heavy metals from contaminated water. Chem. Eng. J. 445, 136513 https://doi.org/10.1016/j.cej.2022.136513.

Sreeram, A., Hadi, P., Hui, C.-W., Al Ansari, T., McKay, G., 2017. Optimisation of the removal of arsenate from water using nanochitosan. Desalin. Water Treat. 70, 235–243. https://doi.org/10.5004/dwt.2017.20561.

Tan, G., Mao, Y., Wang, H., Xu, N., 2020a. A comparative study of arsenic(V), tetracycline and nitrate ions adsorption onto magnetic biochars and activated carbon. Chem. Eng. Res. Des. 159, 582–591. https://doi.org/10.1016/j.cherd.2020.05.011.

Tan, P., Zheng, Y., Hu, Y., 2020b. Efficient removal of arsenate from water by lanthanum immobilized electrospun chitosan nanofiber. Colloids Surf A Physicochem Eng Asp 589, 124417. https://doi.org/10.1016/j.colsurfa.2020.124417.

Tang, H., Zhang, Y., Zhang, Y., Xiao, Q., Zhao, X., Yang, S., 2022. Turning waste into adsorbent: Modification of discarded orange peel for highly efficient removal of Cd (II) from aqueous solution. Biochem. Eng. J. 185, 108497 https://doi.org/10.1016/j.bej.2022.108497.

Thommes, M., Kaneko, K., Neimark, A.V., Olivier, J.P., Rodriguez-Reinoso, F., Rouquerol, J., Sing, K.S.W., 2015. Physisorption of gases, with special reference to the evaluation of surface area and pore size distribution (IUPAC Technical Report). Pure Appl. Chem. 87, 1051–1069. https://doi.org/10.1515/pac-2014-1117.

Vaca-Escobar, K., Villalobos, M., Ceniceros-Gómez, A.E., 2012. Natural arsenic attenuation via metal arsenate precipitation in soils contaminated with metallurgical wastes: III. Adsorption versus precipitation in clean As(V)/goethite/Pb(II)/carbonate systems. Appl. Geochem. 27 (11), 2251–2259. https://doi.org/10.1016/j.apgeochem.2012.01.011.

Vardhan, K.H., Kumar, P.S., Panda, R.C., 2019. A review on heavy metal pollution, toxicity and remedial measures: Current trends and future perspectives. J. Mol. Liq. 290, 111197 https://doi.org/10.1016/j.molliq.2019.111197.

Vinayagam, V., Murugan, S., Kumaresan, R., Narayanan, M., Sillanpää, M., Vo, D.-V.-N., Kushwaha, O.S., 2022. Protein nanofibrils as versatile and sustainable adsorbents for an effective removal of heavy metals from wastewater: A review. Chemosphere 301, 134635. https://doi.org/10.1016/j.chemosphere.2022.134635.

Wang, J., Guo, X., 2020. Adsorption kinetic models: Physical meanings, applications, and solving methods. J. Hazard. Mater. 390, 122156 https://doi.org/10.1016/j.jhazmat.2020.122156.

Wang, Z., Jang, H.M., 2022. Comparative study on characteristics and mechanism of levofloxacin adsorption on swine manure biochar. Bioresour. Technol. 351, 127025 https://doi.org/10.1016/j.biortech.2022.127025.

Wang, Z., Bin Kang, S., Won, S.W., 2022. Polyethylenimine-aminated polyvinyl chloride fiber for adsorption of reactive dyes from single and binary component systems: Adsorption kinetics and isotherm studies. Colloids Surf A Physicochem Eng Asp 647, 128983. https://doi.org/10.1016/j.colsurfa.2022.128983.

Wei, N., Yang, J., Dong, K., Fang, Y., Qin, Z., 2022. Amino-functionalized bovine serum albumin amyloid fibrils aerogel for absorbing copper from water. J. Clean. Prod. 380, 134955 https://doi.org/10.1016/j.jclepro.2022.134955.

Xu, L., Zheng, Y., Zhao, Y., Chen, W., 2023. Recovery of arsenic oxide, harmless gypsum residue and clean water by lime neutralization and precipitation. Hydrometall. 215, 105996 https://doi.org/10.1016/j.hydromet.2022.105996.

Yanti, I., Sationo, P.P., Winata, W.F., Anugrahwati, M., Anas, A.K., Swasono, Y.A., 2023. Effectiveness of activated carbon magnetic composite from banana peel (Musa acuminata) for recovering iron metal ions. Case Studies in Chemical and Environmental Engineering 8, 100378. https://doi.org/10.1016/j.cscee.2023.100378.

Yin, C., Li, S., Liu, L., Huang, Q., Zhu, G., Yang, X., Wang, S., 2021. Structure-tunable trivalent Fe-Al-based bimetallic organic frameworks for arsenic removal from contaminated water. J. Mol. Liq. 346, 117101 https://doi.org/10.1016/J.MOLLIQ.2021.117101.

Zaidi, Z., Sorokhaibam, L.G., 2021. Manganese modified multifunctional carbon material for desulfurization of transportation fuel and CO2 sequestration. J. Environ. Chem. Eng. 9, 105378 https://doi.org/10.1016/j.jece.2021.105378.

Zamora-Ledezma, C., Negrete-Bolagay, D., Figueroa, F., Zamora-Ledezma, E., Ni, M., Alexis, F., Guerrero, V.H., 2021. Heavy metal water pollution: A fresh look about hazards, novel and conventional remediation methods. Environ. Technol. Innov. 22, 101504 https://doi.org/10.1016/J.ETI.2021.101504.

Zhang, C., Fu, Y., Li, Z., Li, T., Shi, Y., Xie, H., Li, Y., Su, H., Li, Z., 2021. Application of whey protein isolate fibrils in encapsulation and protection of β-carotene. Food Chem. 346, 128963 https://doi.org/10.1016/j.foodchem.2020.128963.

Zhang, X., Hao, Y., Wang, X., Chen, Z., 2017. Rapid removal of zinc(II) from aqueous solutions using a mesoporous activated carbon prepared from agricultural waste. Materials 10, 1002. https://doi.org/10.3390/ma10091002.

Zhang, X., Fan, H., Yuan, J., Tian, J., Wang, Y., Lu, C., Han, H., Sun, W., 2022. The application and mechanism of iron sulfides in arsenic removal from water and wastewater: A critical review. J. Environ. Chem. Eng. 10, 108856 https://doi.org/10.1016/j.jece.2022.108856.

Zhang, W., Liu, C., Wang, L., Zheng, T., Ren, G., Li, J., Ma, J., Zhang, G., Song, H., Zhang, Z., Li, Z., 2019. A novel nanostructured Fe-Ti-Mn composite oxide for highly efficient arsenic removal: Preparation and performance evaluation. Colloids Surf A Physicochem Eng Asp 561, 364–372. https://doi.org/10.1016/j.colsurfa.2018.10.077.

Zoroufchi Benis, K., Sokhansanj, A., Norberto, J., McPhedran, K.N., Soltan, J., 2022. A binary oxide-biochar composite for adsorption of arsenic from aqueous solutions: Combined microwave pyrolysis and electrochemical modification. Chem. Eng. J. 446, 137024 https://doi.org/10.1016/j.cej.2022.137024.